Materials Horizons

ROYAL SOCIETY OF CHEMISTRY

COMMUNICATION

View Article Online
View Journal | View Issue

Cite this: *Mater. Horiz.*, 2020, 7, 1310

Received 11th December 2019,
Accepted 24th February 2020

DOI: 10.1039/c9mh01999e

rsc.li/materials-horizons

Selective metathesis synthesis of $MgCr_2S_4$ by control of thermodynamic driving forces†

Akira Miura, *[a] Hiroaki Ito, [b] Christopher J. Bartel, [c] Wenhao Sun, *[de] Nataly Carolina Rosero-Navarro, [a] Kiyoharu Tadanaga, [a] Hiroko Nakata, [f] Kazuhiko Maeda [f] and Gerbrand Ceder[cd]

$MgCr_2S_4$ thiospinel is predicted to be a compelling Mg-cathode material, but its preparation via traditional solid-state synthesis methods has proven challenging. Wustrow *et al.* [*Inorg. Chem.*, 2018, 57, 14] found that the formation of $MgCr_2S_4$ from $MgS + Cr_2S_3$ binaries requires weeks of annealing at 800 °C with numerous intermediate regrinds. The slow reaction kinetics of $MgS + Cr_2S_3 \rightarrow MgCr_2S_4$ can be attributed to a miniscule thermodynamic driving force of $\Delta H = -2$ kJ mol^{-1}. Here, we demonstrate that the double ion-exchange metathesis reaction, $MgCl_2 + 2NaCrS_2 \rightarrow MgCr_2S_4 + 2NaCl$, has a reaction enthalpy of $\Delta H = -47$ kJ mol^{-1}, which is thermodynamically driven by the large exothermicity of NaCl formation. Using this metathesis reaction, we successfully synthesized $MgCr_2S_4$ nanoparticles (<200 nm) from $MgCl_2$ and $NaCrS_2$ precursors in a KCl flux at 500 °C in only 30 minutes. NaCl and other metathesis byproducts are then easily washed away by water. We rationalize the selectivity of $MgCr_2S_4$ in the metathesis reaction from the topology of the DFT-calculated pseudo-ternary $MgCl_2$–$CrCl_3$–Na_2S phase diagram. Our work helps to establish metathesis reactions as a powerful alternative synthesis route to inorganic materials that have otherwise small reaction energies from conventional precursors.

New concepts

Complex inorganic materials are usually synthesized by an 'addition' approach, whereby simple precursors are reacted to form a target multicomponent phase. However, if the simple precursors are already very stable themselves, then there may be little free energy left to drive a chemical reaction to a higher-component phase, which often results in slow kinetics and long-lived reaction impurities. Here, we demonstrate that metathesis reactions operate in a fundamentally different synthesis paradigm. During double ion-exchange metathesis, the inclusion of extra chemical species, such as Na^+ and Cl^-, dramatically changes the thermodynamic topology of the phase diagram. This shifting energy landscape modifies the relevant chemical reactions, intensifies reaction thermodynamics, and can relocate the 'thermodynamic sink' of the phase diagram to a new composition—enhancing structure-selectivity towards a target multicomponent phase. We further demonstrate that candidate metathesis reactions can be rapidly screened and evaluated using publicly available DFT thermochemical data. The additional degrees of freedom afforded by including extra elements into the phase diagram opens up a vast and promising design space for creative new metathesis reactions.

Introduction

Synthesis is the bedrock of inorganic materials chemistry,[1] serving as the first step to any further investigation into the structure–property relationships of materials. For ceramic materials, the traditional approach to solid-state synthesis involves grinding or milling precursors into powder form, followed by the firing of these precursors at high temperatures to form more complex materials. While this approach has led to the synthesis of many inorganic materials, it remains limited by a number of thermodynamic and kinetic constraints.[2] For example, the synthesis temperature should be high enough to facilitate fast diffusion and reaction kinetics, but low enough that the target compound does not melt or decompose. However, high temperatures also lead to the ripening of large particles, which eliminates interfaces and thereby reduces reaction kinetics.[3] Because of these often conflicting constraints, solid-state synthesis occasionally proceeds with slow reaction kinetics, non-equilibrium intermediates, or impurities,[4–6] which hinder the phase-pure synthesis of a desired target material.

One such material that has proven difficult to synthesize via traditional solid-state synthesis is $MgCr_2S_4$ thiospinel. In the search for Mg-ion cathode materials beyond the dominant Chevrel Mo_6S_8 phase,[7] Mg-thiospinels emerged as a promising

[a] *Faculty of Engineering, Hokkaido University, Sapporo 060-8628, Japan. E-mail: amiura@eng.hokudai.ac.jp*
[b] *Graduate School of Chemical Sciences and Engineering, Hokkaido University, Sapporo 060-8628, Japan*
[c] *Department of Materials Science and Engineering, UC Berkeley, Berkeley, California 94720, USA*
[d] *Materials Sciences Division, Lawrence Berkeley National Laboratory, Berkeley, CA 94720, USA*
[e] *Department of Materials Science and Engineering, University of Michigan, Ann Arbor, Michigan, 48109, USA. E-mail: whsun@umich.edu*
[f] *Department of Chemistry, School of Science, Tokyo Institute of Technology, Tokyo 152-8550, Japan*

† Electronic supplementary information (ESI) available: See DOI: 10.1039/c9mh01999e

class of compounds. Thiospinels benefit from a soft sulfur anion sublattice, which enhances Mg-ion mobility compared to oxides, and a spinel framework, which provides a favorable tetrahedral → octahedral → tetrahedral Mg^{2+} migration path with a low diffusion barrier.[8,9] $MgTi_2S_4$ was the first demonstrated Mg-thiospinel cathode material, successfully cycled at a C/5 rate at 60 °C and achieving a specific energy density of 230 W h kg^{-1}.[10,11] Our computational search for other candidate Mg-thiospinels found $MgCr_2S_4$ to possess compelling properties, including a high specific capacity (209 mA h g^{-1}) and energy density (244 W h kg^{-1}), as well as a relatively low Mg-ion diffusion barrier of 540 meV.[10] Notably, $MgCr_2S_4$ was calculated with density functional theory (DFT) to fall upon the Mg–Cr–S convex hull, meaning it is thermodynamically stable with respect to competing compounds and should therefore be synthesizable.

Following this prediction, Wustrow *et al.* successfully synthesized $MgCr_2S_4$ through a traditional solid-state synthesis approach—although it was found to be a laborious reaction.[12] Starting from elemental (Mg + Cr + S) precursors, the binary sulfides, MgS and Cr_2S_3, formed rapidly upon heating. However, the subsequent reaction from MgS + Cr_2S_3 to ternary $MgCr_2S_4$ required holding at 800 °C for two weeks, with numerous intermediate regrinds. Notably, the reaction could not be accelerated by carrying out the synthesis at higher temperatures as $MgCr_2S_4$ decomposes into MgS and Cr_2S_3 above 900 °C. Although $MgCr_2S_4$ is indeed a thermodynamically stable compound, we calculate the driving force (reaction enthalpy, ΔH_r) for its formation from MgS + Cr_2S_3 to be extremely small (−2 kJ mol^{-1}, eqn (1)).

$$MgS + Cr_2S_3 \rightarrow MgCr_2S_4;\ \Delta H_r = -2\ \text{kJ mol}^{-1} \quad (1)$$

All reaction energies in this work utilize the publicly available DFT-calculated thermochemical data in the Materials Project database (Methods). The slow reaction kinetics observed by Wustrow *et al.* can be attributed to this miniscule thermodynamic driving force. Moreover, long synthesis times can lead to the ripening of large $MgCr_2S_4$ particles, which reduces the interfacial area needed to activate Mg-ion intercalation and further slows down the reaction kinetics.

Metathesis reactions offer an intriguing synthesis route to solid-state materials with otherwise small reaction energies. In a metathesis reaction, an alkali or alkaline earth metal compound is combined with a metal halide, which drives a highly exothermic double ion-exchange reaction. For example, a compelling metathesis reaction for $MgCr_2S_4$ can be written as:

$$2NaCrS_2 + MgCl_2 \rightarrow MgCr_2S_4 + 2NaCl;\ \Delta H_r = -47\ \text{kJ mol}^{-1} \quad (2)$$

The >20× increase in thermodynamic driving force from ΔH_r = −2 kJ mol^{-1} to −47 kJ mol^{-1} is because Na^+ and Cl^- are separated in the precursors but rejoined to form the very stable NaCl salt on the product side. Along with a dramatic increase in reaction enthalpy, other advantages afforded by metathesis reactions include faster reaction kinetics and the potential to form nanocrystals and porous materials.[13] Not only can metathesis reactions be used to synthesize stable materials with otherwise small reaction energies, the increased thermodynamic driving force and fast reaction kinetics also affords the synthesis of metastable materials,[14] as were previously demonstrated on nitrides,[13,15–17] sulfides,[13,18,19] and oxides.[20–22] Motivated by the metathesis reaction shown in eqn (2), we designed a two-step sequential metathesis reaction to synthesize $MgCr_2S_4$, as visualized in Scheme 1.

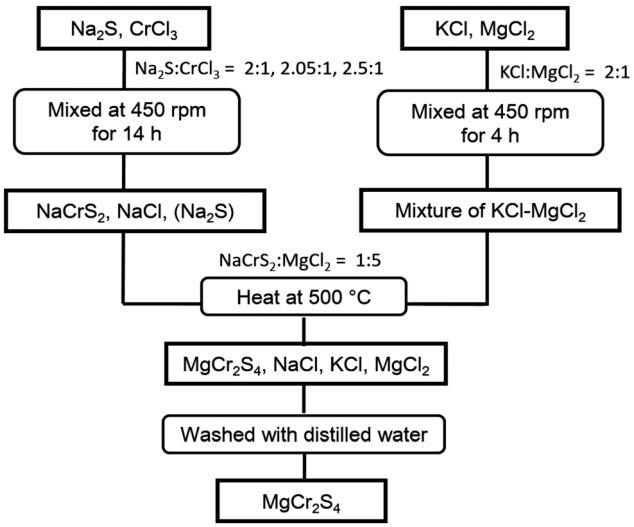

Scheme 1 Two-step metathesis flux synthesis of $MgCr_2S_4$.

Results

In the first reaction, we ball milled $CrCl_3$ and Na_2S to form $NaCrS_2$ (eqn (3)). This reaction is highly exothermic (ΔH_r = −359 kJ mol^{-1}) and proceeds even without external heating.

$$CrCl_3 + 2Na_2S \rightarrow NaCrS_2 + 3NaCl;\ \Delta H_r = -359\ \text{kJ mol}^{-1} \quad (3)$$

To conduct the metathesis reaction described in eqn (2), we next heated the byproducts from eqn (3) in a KCl–$MgCl_2$ flux at 500 °C in nitrogen atmosphere. We prepared the KCl–$MgCl_2$ flux at the eutectic composition of $KCl:MgCl_2 \sim 2:1$, which has a melting point of ∼430 °C.[23]

We chose to conduct the reaction in a mixed chloride flux media because the eutectic temperature of a mixed chloride flux can be relatively low, which provides a liquid reaction media to facilitate fast diffusion kinetics. Here, we considered LiCl, NaCl, and KCl as candidate flux chemistries to mix with $MgCl_2$. We disqualified a LiCl–$MgCl_2$ flux because the ion-exchange reaction of $NaCrS_2$ with LiCl has a favorable driving force to form $LiCrS_2$, which could compete with the formation of $MgCr_2S_4$ (eqn (4)). We also disqualified NaCl–$MgCl_2$ as a potential flux media because NaCl is a byproduct of the metathesis reaction, meaning the NaCl composition of the flux would change as the metathesis reaction proceeds. Any deviation away from the eutectic composition would increase the melting temperature of the NaCl–$MgCl_2$ flux; which, if increased too much, could cause the flux to solidify and thereby disrupt the reaction. KCl–$MgCl_2$ emerges as the ideal flux media, because the formation of $KCrS_2$ from $NaCrS_2$ + KCl is not thermodynamically

favorable (eqn (5)), and the eutectic point of KCl–$MgCl_2$ (~430 °C)[23] is lower than that of NaCl–$MgCl_2$ (~445 °C)[24] Furthermore, the formation of NaCl byproduct in a KCl–$MgCl_2$ flux would actually lower the KCl–$MgCl_2$ eutectic temperature,[24] and thereby would not impede the flux-mediated reaction kinetics.

$$NaCrS_2 + LiCl \rightarrow LiCrS_2 + NaCl;\ \Delta H_r = -16\ kJ\ mol^{-1} \quad (4)$$

$$NaCrS_2 + KCl \rightarrow KCrS_2 + NaCl;\ \Delta H_r = +33\ kJ\ mol^{-1} \quad (5)$$

These reaction thermodynamics are also straightforward to evaluate using the Materials Project Reaction Calculator app, which can help guide the rational design of flux chemistries.

We synthesized $NaCrS_2$ in a reaction between $CrCl_3$ and Na_2S by ball-milling at 450 rpm in a zirconia jar with zirconia milling media. We tried three molar ratios for $CrCl_3 : Na_2S$—1 : 2 (stoichiometric), 1 : 2.05 (2.5% Na_2S excess), and 1 : 2.5 (25% Na_2S excess)—producing $NaCrS_2$ and NaCl (eqn (3)). In the second step, the ball-milled mixture of $NaCrS_2$ and NaCl were placed in a carbon crucible together with the $MgCl_2$–KCl flux at a molar ratio of $NaCrS_2 : MgCl_2$ = 1 : 5. The reaction was performed at 500 °C for 30 minutes in an inert nitrogen atmosphere. After cooling, the synthesized products were washed with distilled water and centrifuged in air to remove the flux and excess $MgCl_2$ and Na_2S. Fig. 1 shows the XRD characterization of the synthesis products. The ball-milling of Na_2S and $CrCl_3$ indeed produced $NaCrS_2$ with NaCl byproduct, as anticipated from eqn (3). The reaction of $NaCrS_2$ + NaCl in a $MgCl_2$–KCl flux resulted in $MgCr_2S_4$, Cr_2S_3 and MgO, where the ratios of these products varied with the Na_2S excess in the precursor (Fig. 1). For a stoichiometric ratio of $CrCl_3 : Na_2S$ = 1 : 2, we observe a coexistence of Cr_2S_3 and $MgCr_2S_4$. When we include Na_2S excess in the synthesis of $NaCrS_2$ (eqn (3)), the Cr_2S_3 impurity from the flux reaction is diminished. With 25% Na_2S excess, the reaction yields nearly phase-pure $MgCr_2S_4$.

All metathesis byproducts and flux media (KCl, NaCl, $MgCl_2$, Na_2S) and any possibly synthesized MgS are soluble in water and were removed from the system by washing with distilled water. Although our final product yields $MgCr_2S_4$ as the dominant phase, it contains MgO as a minor impurity. These reactions were conducted in inert nitrogen atmosphere, suggesting the incorporation of oxygen in MgO may have arisen from washing with water. To examine the effect of washing with water, we performed the same synthesis reaction of $NaCrS_2$ with $MgBr_2$–KBr flux, with excess $MgBr_2$ and Na_2S, and subsequently removed metathesis products by washing with anhydrous methanol. In the $MgBr_2$ synthesis, MgO still forms as an impurity phase, in fact with even larger phase fraction than when synthesized in the $MgCl_2$–KCl flux (Fig. S1, ESI†). This suggests that the oxygen does not originate from the water. Oxygen impurities may have therefore already existed in the $MgCl_2$ or $MgBr_2$ precursors, or from a low but nonzero p_{O_2} and/or p_{H_2O} in the nitrogen atmosphere.

We performed three control experiments to validate the importance of the designed synthesis parameters for the metathesis reaction of $MgCr_2S_4$. In our first control experiment, we reacted the traditional precursors MgS + Cr_2S_3 in a $MgCl_2$–KCl flux at 500 °C for 30 min, and in the second control experiment,

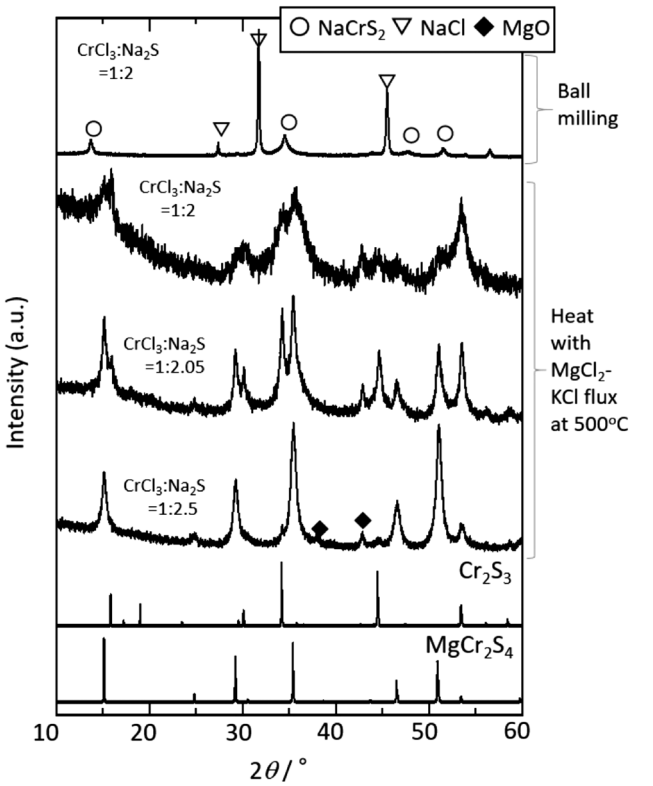

Fig. 1 XRD patterns of $NaCrS_2$ powder synthesized via ball milling from $CrCl_3$ and Na_2S, and $MgCr_2S_4$ powder synthesized by $NaCrS_2$ and $MgCl_2$–KCl flux at 500 °C and subsequent wash with water. Different molar ratios of $CrCl_3 : Na_2S$ were utilized for producing $MgCr_2S_4$.

we reacted $NaCrS_2$ + $MgCl_2$ without the flux at 500 °C for 30 min. Neither of these two control experiments were found to form $MgCr_2S_4$ (Fig. S2 and S3, ESI†). The former reaction supports the importance of metathesis precursors, $NaCrS_2$ + $MgCl_2$, while the latter reaction supports the need for a liquid phase (*i.e.*, $MgCl_2$–KCl flux). For the third control experiment, we reacted $NaCrS_2$ with $MgCl_2$ at 800 °C, where $MgCl_2$ becomes liquid even without KCl (the melting point of $MgCl_2$ is 714 °C).[25] This reaction did form $MgCr_2S_4$, along with Cr_2S_3 impurity (Fig. S3, ESI†). This final control reaction shows that $MgCl_2$ liquid is important for this reaction, and the presence of KCl enables this liquid phase to form well below the $MgCl_2$ melting point, decreasing the required temperature from 714 °C to 430 °C. Together, these experiments show that the rapid synthesis of $MgCr_2S_4$ at 500 °C requires the metathesis precursors ($NaCrS_2$ + $MgCl_2$) and the $MgCl_2$–KCl flux.

Rietveld refinement of $MgCr_2S_4$ synthesized from Na_2S and $MgCl_2$ excess (Fig. 2a) shows that the lattice parameter of $MgCr_2S_4$ is 1.01426(12) nm, agreeing with the previously reported $MgCr_2S_4$ synthesized by high-temperature solid-state synthesis (1.01415(2) nm).[12] Rietveld refinement shows no inversion between Mg and Cr sites in the spinel structure. Fig. 2b shows the STEM images and corresponding EDX mapping of $MgCr_2S_4$ particles synthesized via metathesis reactions with Na_2S and $MgCl_2$ excess. The as-synthesized particles are 50–200 nm in size and 20–50 nm in thickness. The relative surface area of powder

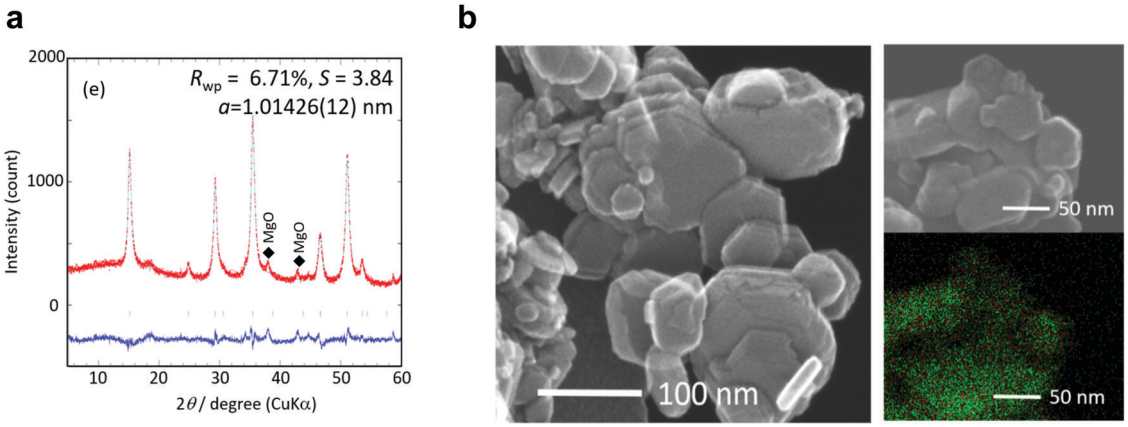

Fig. 2 (a) Rietveld profile of $MgCr_2S_4$ synthesized with excess Na_2S. Residual is shown as the blue line. (b) STEM image of $MgCr_2S_4$ platelet particles. Right side is STEM and EDX mapping: red and green signals represent Mg and Cr signals, respectively.

by N_2 absorption is found to be 55 $m^2\ g^{-1}$. These small $MgCr_2S_4$ particle sizes result from the low temperatures and short reaction times of metathesis synthesis, which quench the nanoparticles shortly after nucleation and before significant crystal growth occurs.[13] This can be contrasted against conventional solid-state synthesis, where high reaction temperatures and long anneal times tend to yield large particle sizes due to Ostwald ripening and particle coarsening during crystal growth.[3,26] The molar ratio of Mg/Cr/S determined by EDX of the product is 1/2.4/4.1, which is close to the stoichiometric ratio of $MgCr_2S_4$. EDX mapping showed homogeneously distributed Mg and Cr, further supporting the formation of $MgCr_2S_4$.

The electronic properties of $MgCr_2S_4$ are an important consideration for Mg-ion battery performance and photochemical applications because Cr_2S_3 has been reported as an n- and p-type semiconductor (band gap, E_g = 0.8 eV).[27] We measured the optical band gap of $MgCr_2S_4$ using diffuse reflectance spectroscopy (ESI†), which we estimate from the Tauc-plot to be 2.2 eV (Fig. S4, ESI†). By means of Mott–Schottky plot analysis (Fig. S5, ESI†), $MgCr_2S_4$ is shown to be an n-type semiconductor with a flat-band potential of *ca.* −0.6 V *vs.* Ag/AgCl at pH 7.0, indicating it is also a candidate H_2 evolution photocatalyst under visible light radiation.[28]

Discussion

The accelerated formation of $MgCr_2S_4$ during metathesis (~30 minutes) compared with solid-state synthesis (~2 weeks) can be rationalized from the thermodynamic topology of each synthesis space. Fig. 3a shows the ternary convex hull phase diagram for Mg–Cr–S, and Fig. 3b shows a pseudo-ternary convex hull phase diagram for $MgCl_2$–$CrCl_3$–Na_2S, which is a slice of the larger 5-component Mg–Cr–S–Na–Cl phase diagram. The colorbar illustrates the 'depth' of the convex hull, corresponding to the reaction energy at each composition relative to the precursor endpoints. Even though $MgCr_2S_4$ has a very favorable formation enthalpy of −1.289 eV $atom^{-1}$, MgS and Cr_2S_3 also have very negative formation enthalpies of −1.76 and −1.097 eV $atom^{-1}$, respectively. In the Mg–Cr–S phase diagram, the deepest point is at the MgS composition, meaning MgS acts as a thermodynamic 'sink' in the traditional ceramic synthesis and explains why MgS tends to persist during the traditional ceramic synthesis. Fig. 3c depicts the tiny energy gain to form $MgCr_2S_4$ along the MgS–Cr_2S_3 reaction tie-line, which further underlies the slow reaction kinetics.

On the other hand, the $MgCl_2$–$CrCl_3$–Na_2S metathesis phase diagram exhibits a qualitatively different thermodynamic topology. Here, each Mg–Cr–S composition must also be accompanied by a stoichiometrically balanced amount of NaCl, which modifies the reaction energies at each composition in the pseudo-ternary space. $MgCr_2S_4$ is balanced by 8NaCl, whereas MgS is balanced by 2NaCl, $NaCrS_2$ by 3NaCl, and Cr_2S_3 by 6NaCl. In the $MgCl_2$–$CrCl_3$–Na_2S phase diagram, the inclusion of NaCl shifts the deepest thermodynamic point from MgS to $MgCr_2S_4$ + Cr_2S_3, which are indeed the observed reaction products in Fig. 1 when synthesized without Na_2S excess. The metathesis route therefore enhances the selective synthesis of $MgCr_2S_4$ by relocating the thermodynamic sink in composition space. Furthermore, because S is tied up with Cr in the $NaCrS_2$ precursor, MgS is unlikely to form in the metathesis reaction, as this would require $NaCrS_2$ decomposition and subsequent reaction of S with the $MgCl_2$ flux.

By increasing the amount of Na_2S excess in the precursor, the diffraction peaks of $MgCr_2S_4$ became dominant and the Cr_2S_3 impurity is eliminated (Fig. 1). This can be rationalized from Le Chatlier's principle, as illustrated in Fig. 3c, where Cr_2S_3 impurities react with excess Na_2S as well as excess $MgCl_2$ from the flux, which further drives the reaction towards the $MgCr_2S_4$ product side. The reaction between Cr_2S_3, $MgCl_2$ and Na_2S (Fig. 3c, orange line) has larger thermodynamic driving force than that between $NaCrS_2$ and $MgCl_2$ (Fig. 3c, blue line). Operating with excess Na_2S and $MgCl_2$ therefore encourages the formation of $MgCr_2S_4$ at the expense of the Cr_2S_3 impurity. Wustrow *et al.* used a similar strategy in the traditional solid-state synthesis route, providing excess MgS to react with Cr_2S_3 impurities in order to achieve high-purity $MgCr_2S_4$.

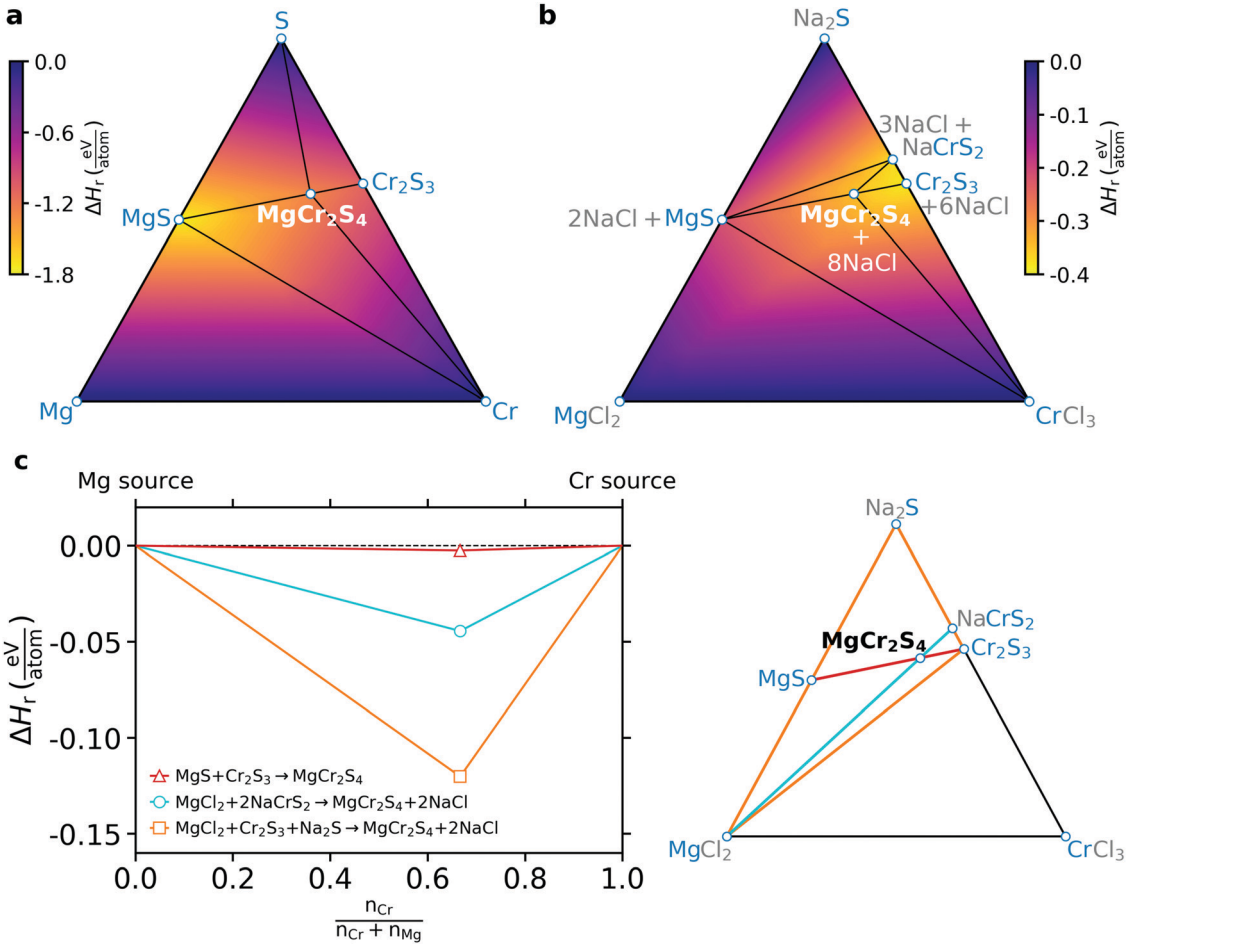

Fig. 3 Ternary phase diagrams for (a) Mg–Cr–S, corresponding to a traditional ceramic synthesis reaction and (b) $MgCl_2$–$CrCl_3$–Na_2S, corresponding to a metathesis reaction. The color bar indicates the reaction enthalpy between the corners of each triangle and the convex hull, which represents the minimum energy phase or mixture of phases at each composition. For (b), ΔH_r is calculated by considering the formation of NaCl where appropriate and therefore is a pseudo-ternary representation of the quinary Mg–Cr–S–Na–Cl chemical space. (c) Driving force for $MgCr_2S_4$ formation from three routes, highlighted by their color in the corresponding pseudo-ternary phase diagram. The reaction relevant to ceramic synthesis (eqn (1)) is shown in red, the metathesis reaction (eqn (3)) is shown in blue, and the reaction that proceeds with excess Na_2S + $MgCl_2$, and consumes impurity Cr_2S_3, is shown in orange.

Conclusions

In summary, we demonstrated metathesis reactions as a powerful synthesis route to inorganic materials with otherwise small thermodynamic driving forces. The formation of NaCl as a byproduct not only increases the reaction enthalpy of forming the target phase, but shifts the topology of the phase diagram, changing the composition of the deepest point of the convex hull and thereby enhancing structure-selectivity. Here, we demonstrated the metathesis synthesis of $MgCr_2S_4$ in only 30 minutes at 500 °C, in contrast to a two-week traditional ceramic synthesis at 800 °C with multiple intermediate regrinds. Furthermore, the synthesized $MgCr_2S_4$ particles were 100–200 nm in size, which is a smaller particle size than would be realized in a direct solid-state ceramic synthesis. Our metathesis synthesis of $MgCr_2S_4$ enables future studies of its electrochemical performance for Mg-battery and photocatalytic applications.

From a more general perspective, the concept of the metathesis reaction broadens how we evaluate synthesis and synthesizability. Traditionally, we take an 'addition' approach to materials synthesis, where one mixes together simple precursors to form a more complex multicomponent material. In the metathesis route, the reactions are driven by stable but removable byproducts, which include but are not limited to alkali metal halides. For example, the reaction of chlorides/oxides with H_2S or NH_3 gas could also be used to synthesize sulfides, oxysulfides, nitrides and oxynitrides by generating HCl/H_2O gas as a byproduct.[29–31] Inclusion of these extra species into the phase diagram provides new degrees of freedom for synthesis design, opening up a vast and promising design space for clever metathesis reactions, which can be rapidly screened and evaluated using publicly available DFT thermochemical data. Creative new precursor combinations are still waiting to be exploited within a metathesis synthesis paradigm, which may currently be overlooked due to preconceived notions about precursor selection.[32]

Methods

The thermodynamics for all reactions discussed in this work are obtained from density functional theory calculations of the

reaction enthalpy, ΔH_r, as calculated using the Reaction Calculator app on the Materials Project database.[33] The deviation between calculated and experimentally obtained ΔH_r for solid-state reactions, such as those discussed in this work, is expected to be on the order of $\sim$5–10 kJ mol^{-1}.[34,35] We note that ΔH calculations do not account for the effects of temperature and entropy on the reaction free energies. For solid-state reactions, the $T\Delta S$ contribution to the free energy is generally negligible when all products and reactants are solids. We demonstrated this by calculating the Gibbs energies of reaction, ΔG_r, at 1000 K for each of the reactions in this work using the model described in ref. 36 (Table S1, ESI†). ΔH_r and ΔG_r (1000 K) are -2 and -9 kJ mol^{-1}, respectively, for eqn (1), and -47 and -50 kJ mol^{-1} for eqn (2).

The syntheses were performed by two-step metathesis reactions. First, the reaction between $CrCl_3$ (99%, Sigma-Aldrich) and Na_2S (Nagao & Co., Ltd) with the molar ratio of 1 : 2, 1 : 2.05 (2.5% Na_2S excess), and 1 : 2.5 (25% Na_2S excess) were performed to produce $NaCrS_2$ and NaCl. This reaction was performed by ball-milling at 450 rpm with zirconia pot and ball. The second step was the reaction of $NaCrS_2$ with $MgCl_2$. This reaction was performed at 500 °C for 30 minutes in an inert atmosphere. The ball-milled mixture of $NaCrS_2$ and NaCl was placed in a carbon crucible together with an $MgCl_2$–KCl flux: $MgCl_2$ (99.9%, Kojundo Chemical Laboratory), KCl (> 99.5%, Wako Chemicals). The molar ratio of $NaCrS_2$ to $MgCl_2$ was 1 : 5. After cooling, the synthesized products were washed with distilled water and centrifuged in ambient atmosphere to remove flux and excess $MgCl_2$ and Na_2S. XRD diffraction was measured by MiniFlex 600 (Rigaku). Composition ratio was determined by EDX equipped by scanning electron microscopy (SEM: TM3030). Morphology was observed by scanning transmission electron microscopy (STEM: Hitachi HD-2000). The diffuse reflectance spectra of $MgCr_2S_4$ were measured using a UV-vis spectrophotometer (JASCO V-750) at room temperature. Mott–Schottky plot measurements were conducted using an ALS760Es electrochemical analyzer (BAS) at room temperature. The electrochemical cell was made of Pyrex glass and was a three-electrode-type system using Pt wire and an Ag/AgCl electrode (in saturated KCl aqueous solution) as the counter and reference electrodes, respectively. The pH of the electrolyte solution was adjusted to be 7.0 by mixing $NaH_2PO_4{\cdot}2H_2O$ (99.0–102.0%, Kanto Chemical) and $Na_2HPO_4{\cdot}12H_2O$ (> 99.0%, Kanto Chemical), while keeping the total phosphate concentration of 0.1 M.

Conflicts of interest

There are no conflicts to declare.

Acknowledgements

We thank Nagao & Co., Ltd for providing Na_2S. This work was supported as part of the Joint Center for Energy Storage Research (JCESR), an Energy Innovation Hub funded by the U.S. Department of Energy, Office of Science, Basic Energy Sciences (CJB, WS, GC). This research was partially supported by KAKENHI Grant Numbers JP16H06441 (KM), JP16K21724 (AM), JP17H04950 (AM), and JP19H04682 (AM).

References

1 M. G. Kanatzidis, K. R. Poeppelmeier, S. Bobev, A. M. Guloy, S.-J. Hwu, A. Lachgar, S. E. Latturner, R. E. Schaak, D.-K. Seo, S. C. Sevov, A. Stein, B. Dabrowski, J. E. Greedan, M. Greenblatt, C. P. Grey, A. J. Jacobson, D. A. Keszler, J. Li, M. A. Subramanian, Y. Xia, T. Cagin, U. Häussermann, T. Hughbanks, S. D. Mahanti, D. Morgan, D.-K. Seo, N. A. Spaldin, W. E. Buhro, D. E. Giammar, J. A. Hollingsworth, D. C. Johnson, A. J. Nozik, X. Peng, R. L. Bedard, N. E. Brese, G. Cao, S. S. Dhingra, C. R. Kagan, D. B. Mitzi, M. J. Geselbracht, G. C. Lisensky, M. W. Lufaso, P. A. Maggard, O. K. Michael, A. P. Wilkinson, H.-C. zur Loye, T. Egami, J. E. Greedan, J. P. Hodges, J. D. Martin, J. B. Parise, B. H. Toby, T. A. Vanderah, P. C. Burns, J. Y. Chan, A. E. Meyer, C. B. Murray, A. P. Ramirez, M. D. Ward, L. Yu, M. A. Alario-Franco, P. D. Battle, T. Bein, C. L. Cahill, P. S. Halasyamani, A. Maignan and R. Seshadri, *Prog. Solid State Chem.*, 2008, **36**, 1–133.
2 F. J. DiSalvo, *Science*, 1990, **247**, 649–655.
3 R. M. German, in *Encyclopedia of Materials: Science and Technology*, ed. K. H. J. Buschow, R. W. Cahn, M. C. Flemings, B. Ilschner, E. J. Kramer, S. Mahajan and P. Veyssière, Elsevier, Oxford, 2001, pp. 8641–8643.
4 D. P. Shoemaker, Y.-J. Hu, D. Y. Chung, G. J. Halder, P. J. Chupas, L. Soderholm, J. F. Mitchell and M. G. Kanatzidis, *Proc. Natl. Acad. Sci. U. S. A.*, 2014, **111**, 10922.
5 Z. Jiang, A. Ramanathan and D. P. Shoemaker, *J. Mater. Chem. C*, 2017, **5**, 5709–5717.
6 A. S. Haynes, C. C. Stoumpos, H. Chen, D. Chica and M. G. Kanatzidis, *J. Am. Chem. Soc.*, 2017, **139**, 10814–10821.
7 D. Aurbach, Z. Lu, A. Schechter, Y. Gofer, H. Gizbar, R. Turgeman, Y. Cohen, M. Moshkovich and E. Levi, *Nature*, 2000, **407**, 724–727.
8 Z. Rong, R. Malik, P. Canepa, G. Sai Gautam, M. Liu, A. Jain, K. Persson and G. Ceder, *Chem. Mater.*, 2015, **27**, 6016–6021.
9 M. Liu, Z. Rong, R. Malik, P. Canepa, A. Jain, G. Ceder and K. A. Persson, *Energy Environ. Sci.*, 2015, **8**, 964–974.
10 M. Liu, A. Jain, Z. Rong, X. Qu, P. Canepa, R. Malik, G. Ceder and K. A. Persson, *Energy Environ. Sci.*, 2016, **9**, 3201–3209.
11 X. Sun, P. Bonnick, V. Duffort, M. Liu, Z. Rong, K. A. Persson, G. Ceder and L. F. Nazar, *Energy Environ. Sci.*, 2016, **9**, 2273–2277.
12 A. Wustrow, B. Key, P. J. Phillips, N. Sa, A. S. Lipton, R. F. Klie, J. T. Vaughey and K. R. Poeppelmeier, *Inorg. Chem.*, 2018, **57**, 8634–8638.
13 J. B. Wiley and R. B. Kaner, *Science*, 1992, **255**, 1093–1097.
14 W. Sun, S. T. Dacek, S. P. Ong, G. Hautier, A. Jain, W. D. Richards, A. C. Gamst, K. A. Persson and G. Ceder, *Sci. Adv.*, 2016, **2**, e1600225.
15 J. Odahara, W. Sun, A. Miura, N. C. Rosero-Navarro, M. Nagao, I. Tanaka, G. Ceder and K. Tadanaga, *ACS Mater. Lett.*, 2019, **1**, 64–70.

16 A. Miura, C. Rosero-Navarro, Y. Masubuchi, M. Higuchi, S. Kikkawa and K. Tadanaga, *Angew. Chem., Int. Ed.*, 2016, **55**, 7963–7967.
17 E. G. Rognerud, C. L. Rom, P. K. Todd, N. R. Singstock, C. J. Bartel, A. M. Holder and J. R. Neilson, *Chem. Mater.*, 2019, **31**, 7248–7254.
18 A. J. Martinolich, J. A. Kurzman and J. R. Neilson, *J. Am. Chem. Soc.*, 2016, **138**, 11031–11037.
19 A. J. Martinolich and J. R. Neilson, *Chem. Mater.*, 2017, **29**, 479–489.
20 R. D. Shannon, D. B. Rogers and C. T. Prewitt, *Inorg. Chem.*, 1971, **10**, 713–718.
21 P. K. Todd and J. R. Neilson, *J. Am. Chem. Soc.*, 2019, **141**, 1191–1195.
22 P. K. Todd, A. M. M. Smith and J. R. Neilson, *Inorg. Chem.*, 2019, **58**, 15166–15174.
23 O. Menge, *Z. Anorg. Chem.*, 1911, **72**, 162–218.
24 E. Jänecke, *Z. Anorg. Chem.*, 1950, **261**, 213–225.
25 D. R. Lide, *CRC Handbook of Chemistry and Physics, 84th Edition*, CRC Press, 2003.
26 L. Ratke and P. W. Voorhees, *Growth and Coarsening: Ostwald Ripening in Materials Processing*, Springer-Verlag, 2002.
27 A. Anedda, E. Fortin, F. Ledda and A. Serpi, *Phys. Status Solidi B*, 1982, **114**, K143–K146.
28 K. Maeda, R. Abe and K. Domen, *J. Phys. Chem. C*, 2011, **115**, 3057–3064.
29 S. H. Elder, L. H. Doerrer, F. J. Disalvo, J. B. Parise, D. Guyomard and J. M. Tarascon, *Chem. Mater.*, 1992, **4**, 928–937.
30 A. Miura, K. Tadanaga, E. Magome, C. Moriyoshi, Y. Kuroiwa, T. Takahiro and N. Kumada, *J. Solid State Chem.*, 2015, **229**, 272–277.
31 H. Kageyama, K. Hayashi, K. Maeda, J. P. Attfield, Z. Hiroi, J. M. Rondinelli and K. R. Poeppelmeier, *Nat. Commun.*, 2018, **9**, 772.
32 X. Jia, A. Lynch, Y. Huang, M. Danielson, I. Lang'at, A. Milder, A. E. Ruby, H. Wang, S. A. Friedler, A. J. Norquist and J. Schrier, *Nature*, 2019, **573**, 251–255.
33 A. Jain, S. P. Ong, G. Hautier, W. Chen, W. D. Richards, S. Dacek, S. Cholia, D. Gunter, D. Skinner, G. Ceder and K. A. Persson, *APL Mater.*, 2013, **1**, 011002.
34 C. J. Bartel, A. W. Weimer, S. Lany, C. B. Musgrave and A. M. Holder, *npj Comput. Mater.*, 2019, **5**(1), 4.
35 G. Hautier, S. P. Ong, A. Jain, C. J. Moore and G. Ceder, *Phys. Rev. B: Condens. Matter Mater. Phys.*, 2012, **85**(15), 155208.
36 C. J. Bartel, S. L. Millican, A. M. Deml, J. R. Rumptz, W. Tumas, A. W. Weimer, S. Lany, V. Stevanovic, C. B. Musgrave and A. M. Holder, *Nat. Commun.*, 2018, **9**, 4168.

